

Comparison of Load Capacity and Inductance for Common Active Magnetic Bearings Designs

Timothy Dimond^{1,a}, Robert Rockwell, JR.^{1,b}, Gregory Simmons^{2,c},
Paul Allaire^{1,d}

¹Rotating Machinery and Controls Laboratory, Department of Mechanical and Aerospace Engineering,
University of Virginia, 122 Engineer's Way, Charlottesville,
VA 22904-4746, USA

²Department of Machine Elements, Luleå University of Technology 97187 LULEÅ, Sweden
^atwd5c@virginia.edu, ^brockwell@virginia.edu, ^cgregory.simmons@ltu.se,
^dpea@virginia.edu

Abstract: Active magnetic bearings have become more popular as an alternative to fluid-film or rolling element bearings in rotating machinery. They have also become a method for force excitation for rotordynamic experiments, including system identification experiments. The current work considers alternate active magnetic bearing designs for a fluid film bearing test rig. The three designs considered include a conventional 8-pole design with equal widths, a 12-pole bearing with e-core quadrants, and a 16-pole alternate with two exterior auxiliary poles and two interior main poles per quadrant. Several previous studies have considered equal pole widths in optimizing magnetic bearing stator geometry. While not an optimization study, this analysis presents a comparison of popular AMB geometries commonly used in industrial applications. The load capacity, magnetic field energy, and inductance were compared. The 16-pole bearing was shown to have the highest load capacity of the three designs. The inductive load also increased with increasing number of poles. The 12 and 16 pole designs, with reduced auxiliary pole width, also exhibited better containment of the magnetic flux within each active magnetic bearing quadrant, which simplifies the control problem. The results are of use for AMB designers and provide guidance for future stator optimization studies.

Keywords: Active Magnetic Bearings, Load Capacity, Inductance

Introduction

Active magnetic bearings (AMBs) have become more popular in support and stabilization of rotating machinery [1]. AMBs are a non-contact method of support for rotors. Because of this feature, AMBs have become an attractive method for applying non-contact loading for rotordynamic testing, e.g. [2, 3]. In this load cell application, the AMB can be used to estimate force input to the rotor, either through circuit models or through instrumentation such as Hall sensors [4, 5] or fiber optic strain gages [6].

The present work considers three alternative AMB designs intended for a fluid film journal bearing test rig at Luleå University of Technology, Luleå, Sweden. A schematic of the test rig is shown in Figure 1. The test rig intent is to perform tribological testing of fixed geometry journal bearings. The bearing application is in hydroelectric power generators. To simulate the bearing specific loads, high AMB force output of at least 50 kN per actuator is required.

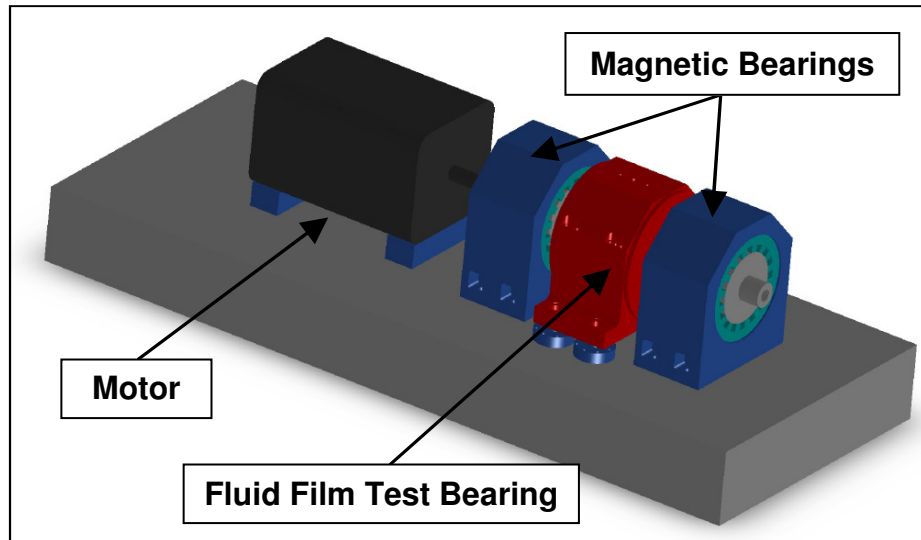


Figure 1. Luleå Test Rig Layout

Most of the prior work on AMB stator geometry reported in the literature has been in the area of optimization of overall AMB systems, where the stator geometry is included in the overall optimization. Recent work on this topic includes use of genetic algorithms to optimize AMBs. Carlson-Skalak et al. [7] used genetic algorithms to optimize eight-pole heteropolar bearings with equal pole widths. The bearings were optimized for maximum RMS load capacity and minimum weight in separate optimizations. The optimizations were constrained by maximum stator outside diameter, journal diameter, axial length, required slew rate, and axial gap. The algorithm was based on catalog selections of standard components, including off-the-shelf amplifiers, sensors, and standard copper wires sizes. Genetic algorithms were also used to optimize eight-pole AMBs with equal pole widths by Chang and Chung [8]. The optima were not constrained by off-the-shelf parts, but were constrained by maximum flux density, closed loop equivalent stiffness assuming PID control, control currents, maximum slew rate, and overall plant stability. The optimization objective was minimum bearing volume.

Stumberger et al. optimized AMBs using the finite element method and the Differential Evolution algorithm [9]. The optimization objective was to produce maximum bearing force for a minimum bearing mass. Again the optimization was limited to eight-pole heteropolar bearings with equal pole width.

Chen and Hsu optimized a three-pole AMB and compared results to a conventional eight-pole AMB [10]. The optimization goal was to minimize copper resistive losses for a given load capacity. Optimization of the coil resistive losses was based on analytical solutions for resistive losses and Lagrange multipliers.

The above studies have concentrated on stator designs with equal pole widths. However, another popular configuration for AMBs is the “e-core” design, where there is one larger central main pole and two smaller auxiliary poles per quadrant [11]. The e-core configuration and a variant, with two larger central main poles and two smaller auxiliary poles per quadrant are used widely by commercial AMB manufacturers.

In the present study, three heteropolar active magnetic bearing designs were considered. The first is an eight-pole bearing with equal pole widths. The second is a 12-pole bearing, with an e-core configuration with one larger central main pole and two smaller auxiliary poles per quadrant. The third is a 16 pole configuration, with two larger central main poles and two smaller auxiliary poles per quadrant. In both the 12-pole and 16-pole configurations, the auxiliary poles were half the width of the main poles. The load capacity, stored magnetic energy, and inductance were compared. This type of comparative study between different popular magnetic bearing stator

geometries is new in the literature. While not an optimization study, it does point to the value of relaxing the equal leg width assumption in performing bearing optimizations.

Design Comparison

The performance of three three heteropolar AMB designs was compared. Due to the high loads required, iron-cobalt-vanadium (FeCoV) alloy material was considered in the analysis. The journal diameter was limited to a maximum of 228.6 mm based on commercially available material. To allow for direct comparison of the designs, the stator outer diameter at 342.9 mm, the bearing axial length at 228.6 mm, the shaft diameter at 228.6 mm and the nominal air gap between rotor and stator at 76 μm were all held constant for all three designs. The poles were arranged into quadrants, and the windings of the poles within each quadrant were treated as connected in series in each design case.

Analysis

The bearing analysis was conducted in two parts. The initial designs were obtained assuming linear magnetic circuit theory. Then, the analyses were confirmed using non-linear finite element analysis (FEA) performed with a commercial code and included saturation effects in the magnetic materials.

Linear Circuit Models. The equations for the linear magnetic circuit models presented are available in [12]. For this analysis, a limiting magnetic flux of 2.2 T was assumed for the magnetic material, which is the knee flux (linear B-H flux limit) for FeCoV alloy. It is assumed that magnetic flux loops are contained within a single quadrant of each AMB design. A typical circuit model for a single quadrant of the 12-pole e-core configuration is shown in Fig. 2.

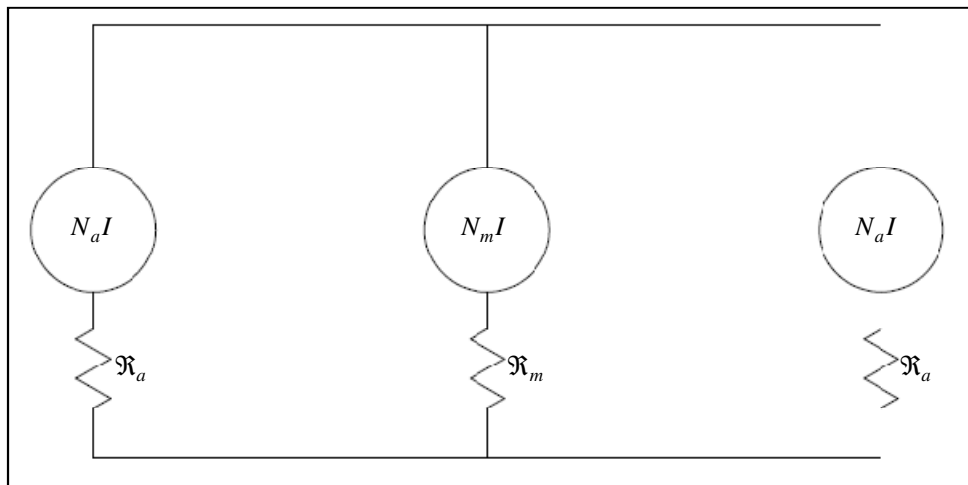


Figure 2. Circuit Model, 12-pole e-core Bearing, Single Quadrant

The fundamental equations for magnetic circuit analysis are Ampere's loop law and conservation of magnetic flux. Ampere's loop law describes the induced magnetic field due to an applied current in a wire coiled around magnetic material and is given by:

$$\sum_{i=1}^{n_s} \left(\frac{Bg}{\mu} \right)_i = \sum_{i=1}^{n_c} (NI)_i \quad (1)$$

Conservation of magnetic flux indicates that the total flux through a node in the magnetic circuit is zero:

$$\sum_{i=1}^{n_p} \Phi_i = 0 \quad (2)$$

The available force was obtained in terms of the peak magnetic flux density for a lumped model as:

$$\mathbf{F} = \frac{A_p B^2}{2\mu_0} \mathbf{n} . \quad (3)$$

The vector \mathbf{n} is a unit normal to the pole face area. The pole face area was limited by the back iron cross-sectional area and the stator inner and outer diameters. The back iron was sized to saturate at the same input current density as the poles.

The slew rate was calculated in terms of linearized bearing operation for opposing quadrants of the AMB designs in the circuit models as:

$$\frac{dF}{dt} = \frac{A\mu_0 N^2 I_b}{2g} \frac{dI_p}{dt} . \quad (4)$$

The inductance for the linear analysis was found as:

$$L = \frac{\mu_0 A_p N^2}{2g} . \quad (5)$$

Equations (1-5) were used to size the AMBs, including individual pole widths, back iron flux paths, nominal air gap, and number of windings for each pole.

Finite Element Analysis. Confirmation of the design alternatives was then performed using commercial finite element software. The finite elements used were 8-node quadrilateral elements. A two-dimensional static non-linear analysis was performed. The analysis assumes that the solution does not vary axially. Material properties, including B-H curves with saturation effects for FeCoV alloy, were modeled explicitly.

The finite elements implement the fundamental constitutive electromagnetic relations in a discretized form. The fundamental relationships are a subset of Maxwell's equations and include magnetomotive, given by:

$$\nabla \times \mathbf{H} = \mathbf{J} \quad (6)$$

The conservation of magnetic flux at a given cross-sectional area in the bearing in differential form is expressed as:

$$\nabla \cdot \mathbf{B} = 0 \quad (7)$$

The applied force from the magnetic fields developed in the AMB and directed through the air gaps is given by

$$\mathbf{f} = \oint \mathbf{T} \cdot d\mathbf{S} \quad (8)$$

The term \mathbf{T} in Eq. (8) is the Maxwell stress tensor, expressed using indicial notation as

$$T_{ij} = \frac{1}{\mu_0} \left(B_i B_j - \frac{1}{2} \delta_{ij} B_{ij}^2 \right) \quad (9)$$

For finite element models of AMBs, the inductance can be calculated using the magnetic energy calculated for the bearing as [13, 14]:

$$L = \frac{2W}{I^2}. \quad (10)$$

Individual finite element meshes were developed for each AMB configuration. The meshes for the 8-pole and 12-pole AMB configurations consisted of approximately 52,000 elements and 155,000 nodes. The mesh for the 16-pole AMB configuration consisted of approximately 60,000 elements and 179,000 nodes. The meshes are provided in Figure 3 for the 8-pole bearing, Figure 4 for the 12-pole bearing, and Figure 5 for the 16-pole bearing. In all of the figures, blue elements represent air, red elements represent the copper windings, cyan elements represent the FeCoV alloy, and magenta elements represent plain carbon steel.

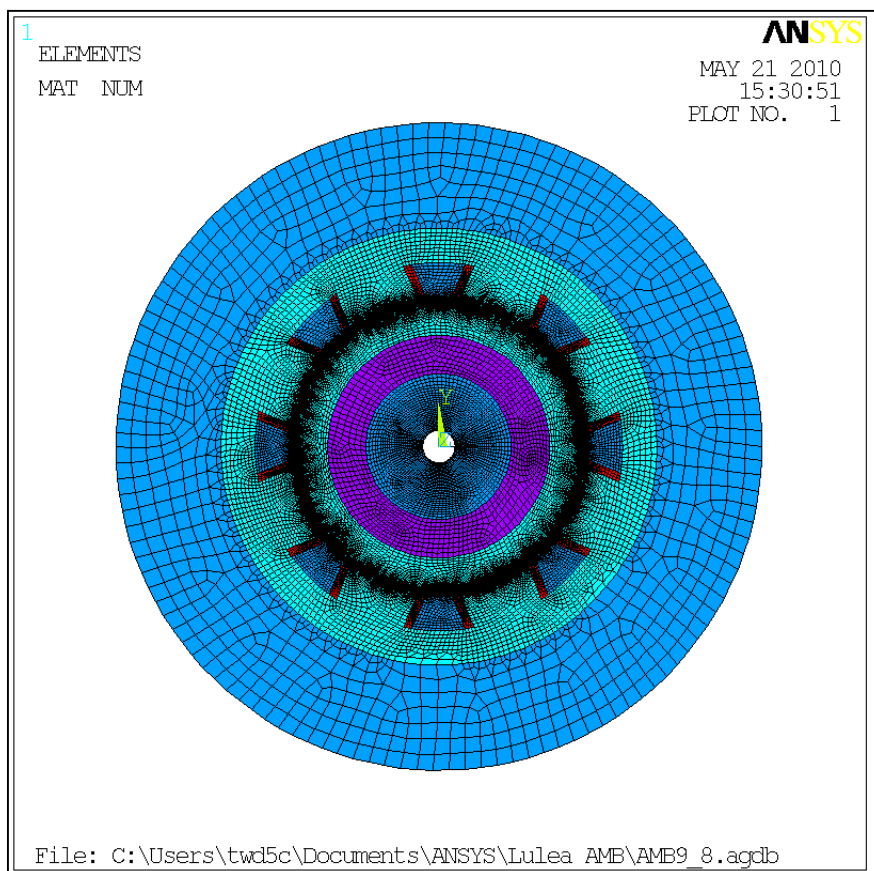


Figure 3. Finite Element Mesh, Conventional 8-pole Bearing

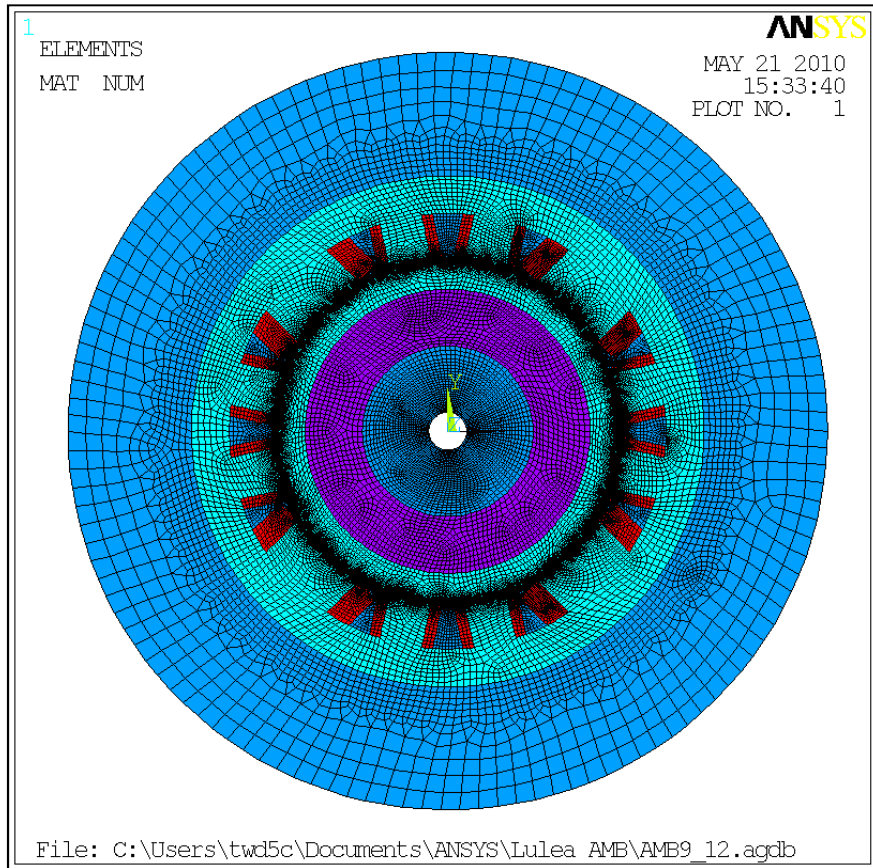


Figure 4. Finite Element Mesh, 12-pole e-core Bearing

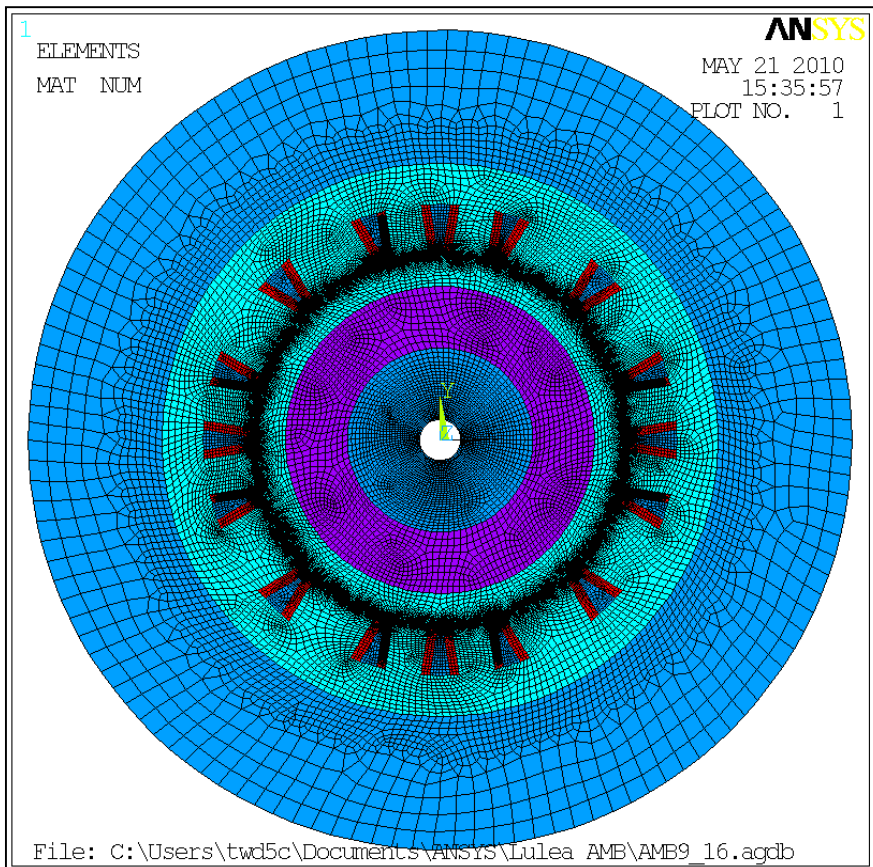


Figure 5. Finite Element Mesh, 16-pole Bearing

Results

The calculated load capacities and inductances for the alternative AMB designs based on magnetic circuit modeling is presented first. The finite element analysis results for the designs obtained using the magnetic circuit models are presented next, and are compared to the linear circuit models.

Magnetic Circuit Model Results. The face area for each pole was restricted by the requirements that the back iron saturate at the same time that the bearing poles and the constraints on stator inner and outer diameters. Based on the geometry constraints, the pole face area per quadrant was approximately the same for the 8-pole and 12-pole configurations. The total pole face area per quadrant was $2.61 \cdot 10^{-2} \text{ m}^2$. As a result, the 8-pole and 12-pole bearings had similar load capacity based on the circuit models. The conventional eight-pole bearing was predicted to have a maximum load capacity of 46.5 kN assuming linear operation. The 12-pole bearing also was predicted to have a maximum load capacity of 46.5 kN. The geometry constraints allowed additional pole face area for the 16-pole configuration. The total pole face area for the 16-pole configuration was $3.05 \cdot 10^{-2} \text{ m}^2$. With the increased pole face area, the 16-pole bearing was predicted to have a maximum load capacity of 53.8 kN. All load capacities are based on a single active quadrant.

The bearing inductance is a function of the number of wiring turns required to obtain the total input current for the bearing quadrant. In all cases, a peak input current (perturbation plus bias) of 60 A was assumed. For the 8-pole bearing, an input of 1334 amp-turns is required to obtain the saturation flux of 2.2 T. The peak input current results in 22 turns of copper wire. The resulting inductance for the 8-pole bearing was 10.4 mH. The 12-pole bearing required a total of 2668 amp-turns and a total of 44 turns of wire. The resulting inductance for the 12-pole bearing was 21.3 mH. The 16-pole bearing also required 2668 amp-turns of current. However, the additional pole increased the total inductance of the 16-pole bearing to 32.4 mH.

Finite Element Analysis Results. Flux line plots are provided for the alternate bearing designs. Figure 6 represents the magnetic flux paths for the 8-pole bearing with equal widths. Figure 7 represents the magnetic flux paths for the 12-pole e-core bearing. Figure 8 represents the magnetic flux paths for the 16-pole bearing.

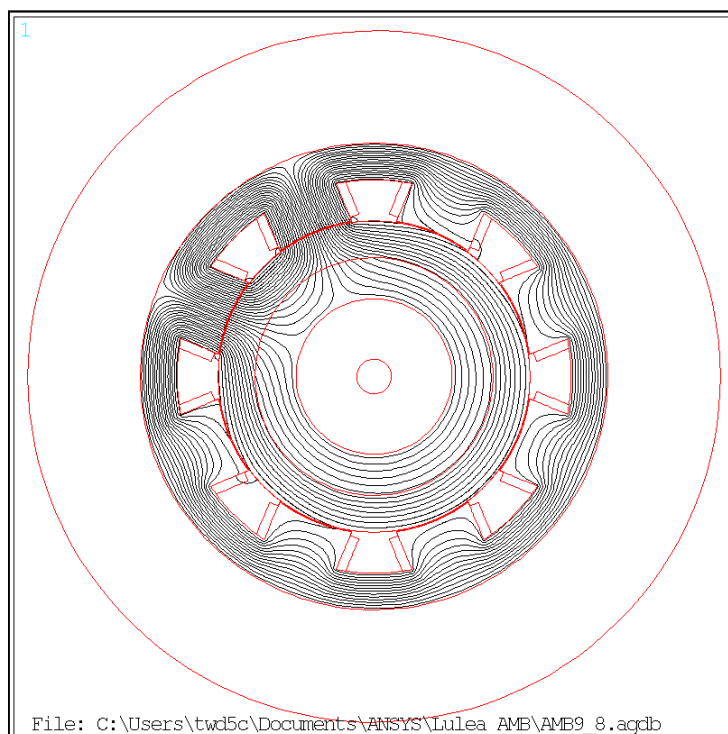


Figure 6. Conventional 8-pole Bearing Magnetic Flux Lines

In Figure 1, the copper windings about the upper left poles are active. The magnetic flux has two alternate paths that it follows. The first is the loop in the active poles. The second is along the back iron. This configuration allows for significant flux leakage.

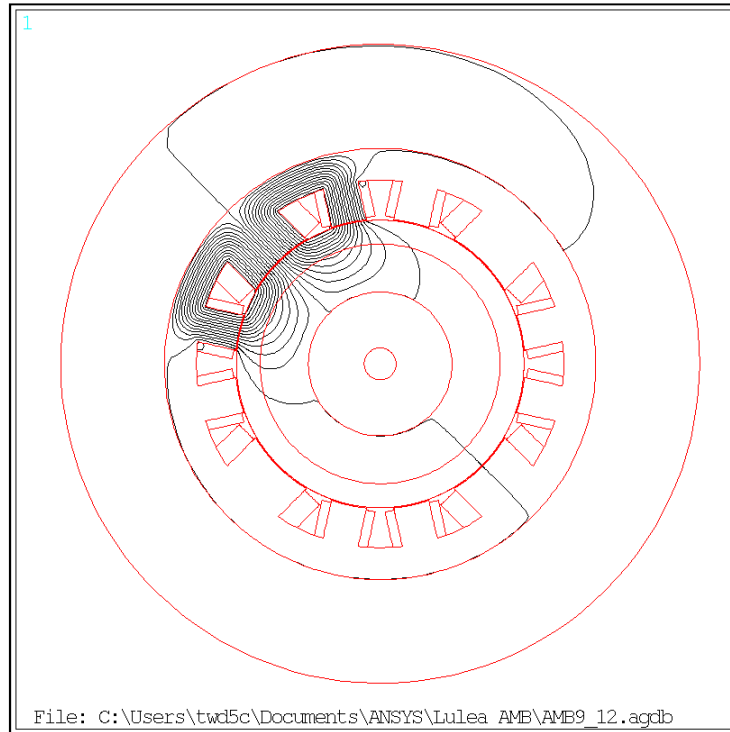


Figure 7. 12 pole Bearing Magnetic Flux Lines

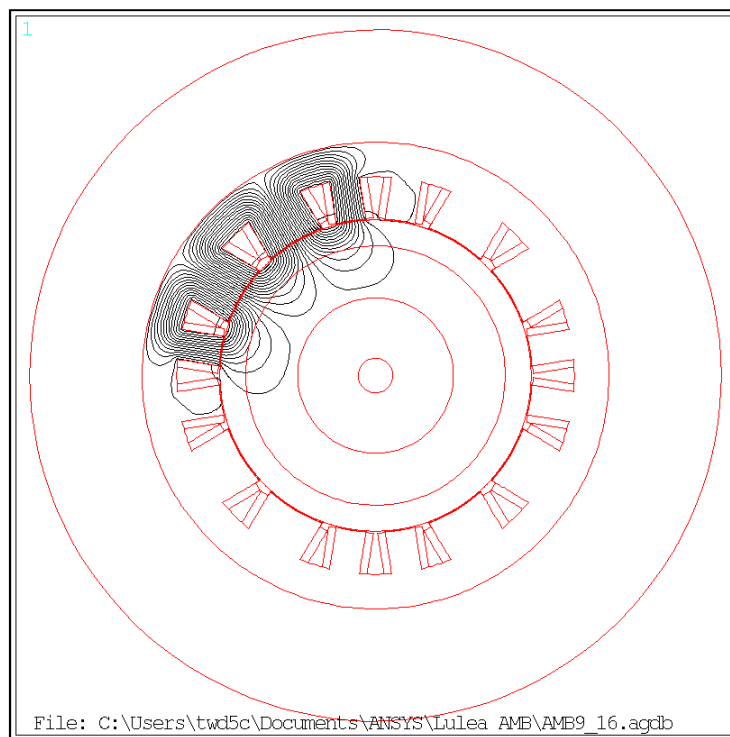


Figure 8. 16-pole Bearing Magnetic Flux Lines

In Figures 7 and 8, the upper left quadrant is again the active quadrant. In these designs, the magnetic flux is well-contained within the quadrant, with minimal leakage to alternate paths.

Table 2 shows the comparison of load capacity, magnetic field energy, and inductance for three heteropolar bearing designs based on the linear circuit model and FEA. The inductance is based on a peak current (bias plus perturbation) of 60 A. The analysis assumes that current is supplied to one quadrant of the bearing, while current is not supplied to the remaining three quadrants. While not practical for normal operation, this assumption allows for direct comparison between designs.

Table 2. Comparison of AMB Designs

Bearing Type	Circuit Model		Finite Element Analysis		
	Force, kN	Inductance, mH	Force, kN	Magnetic Energy, J	Inductance, mH
8	46.5	10.4	37.0	34.1	18.9
12	46.4	21.3	40.7	38.9	21.6
16	53.8	32.4	44.2	40.9	22.7

Discussion and Conclusions

When the linear circuit models are considered, the single quadrant load capacity between the 8-pole and 12-pole bearings was essentially the same, since the total pole face area per quadrant was approximately the same. The 16-pole bearing had a 16 percent increase in load capacity compared to the 8-pole and 12-pole designs. This is due to the increased amount of pole face area, which could be achieved due to the constraints on stator inner and outer diameters. The bearing inductance doubled when the number of poles was increased from 8 to 12, and increased by an additional 50 percent when the number of poles was increased from 12 to 16. The linear magnetic circuit model indicates that for a given amplifier and controller, the frequency bandwidth of the actuator decreases substantially as the number of poles is increased.

When the finite element models are considered, there is a 10 percent increase in load capacity when increasing the number of poles from 8 to 12, and another 10 percent increase in load capacity when increasing the number of poles from 12 to 16. Additionally, the 16-pole bearing exhibits better containment of the magnetic flux, which reduces cross-coupling between quadrants and simplifies the control problem. The inductance increased 11 percent when the number of poles was increased from 8 to 12, but only increased 2 percent when the number of poles was increased from 12 to 16. The increased number of poles gave a higher load capacity without a large penalty in open-loop inductance. The prediction of open-loop inductance indicates that the linear circuit model overpredicts the trend in bandwidth penalty as compared to the finite element model. This phenomenon is of interest to AMB designers looking to improve load capacity and use magnetic material efficiently while limiting inductive load.

When the stator inner and outer diameters are constrained as in this study, the increase in load capacity results from the additional pole face area that can be obtained with the increase in number of poles per quadrant. This information can also be used to improve AMB design optimizations by relaxing the requirement from previous studies that all poles have equal width.

References

- [1] P.E. Allaire, E.H. Maslen, R.R. Humphris, in: *CRC Handbook of Lubrication Technology*, "Magnetic Bearings," CRC Press, Boca Raton, FL (1994), pp. 577-600.
- [2] M. Aenis, E. Knopf, and R. Nordmann: *Mechatronics*, Vol. 12 (2002), pp. 1011-1021.
- [3] T. Dimond, R.D. Rockwell, Jr., P.N. Sheth, P.E. Allaire: "A New Fluid Film Bearing Test Rig for Oil and Water Bearings," *ASME Turbo Expo* (2008), pp. 1101-1110.

- [4] E. Knopf and R. Nordmann: "Identification of the dynamic characteristics of turbulent journal bearings using active magnetic bearings," Proc. 7th International Conference on Vibrations in Rotating Machinery (2000), pp. 381-390.
- [5] K. Kjølhede and I.F. Santos: J. Eng. Gas Turbines Power Vol. 129 (2007), pp. 503-510.
- [6] Z.S. Zutavern and D.W. Childs: J. Eng. Gas Turbines Power Vol. 130 (2008), p. 022504.
- [7] S. Carlson-Skalak, E. Maslen, and Y. Teng: J. Eng. Design Vol. 10 (1999), pp. 143-164.
- [8] H. Chang and S. Chung: Mechatronics Vol. 12 (2002), pp. 19-36.
- [9] G. Stumberger, D. Dolinar, and U. Palmer: IEEE Trans. Magn. Vol. 36 (2000), pp. 1009-1013.
- [10] S. Chen and C. Hsu: IEEE Trans. Magn. Vol. 38 (2002), pp. 3458-3466.
- [11] G. Schweitzer and E.H. Maslen: *Magnetic bearings: theory, design, and application to rotating machinery* (Springer, Dordrecht ; New York, 2009),.
- [12] E. Maslen: *Magnetic Bearings* (2000).
- [13] R. Escarela-Perez, E. Campero-Littlewood, and M.A. Arjona-Lopez: IEEE Proceedings Elec. Power Applications Vol. 152 (2005), pp. 855-861.
- [14] T. W. Nehl, F.A. Fouad, and N.A. Demerdash: IEEE Trans. Power Apparatus Syst. Vol. PAS-101 (1982), pp. 4441-4451.